

PocketNet: A Smaller Neural Network for 3D Medical Image Segmentation

Adrian Celaya^{1,2}, Jonas Actor^{1,2}, Rajarajeswari Muthusivarajan¹, Evan Gates¹, Caroline Chung¹, Dawid Schellingerhout¹, Beatrice Riviere², and David Fuentes¹

¹ The University of Texas MD Anderson Cancer Center, Houston TX 77030

² Rice University, Houston TX 77003

Abstract. Overparameterized deep learning networks have shown impressive performance in the area of automatic medical image segmentation. However, they achieve this performance at an enormous cost in memory, runtime, and energy. A large source of overparameterization in modern neural networks results from doubling the number of feature maps with each downsampling layer. This rapid growth in the number of parameters results in network architectures that require a significant amount of computing resources, making them less accessible and difficult to use. By keeping the number of feature maps constant throughout the network, we derive a new CNN architecture called PocketNet that achieves comparable segmentation results to conventional CNNs while using less than 3% of the number of parameters.

Keywords: Deep learning · Image segmentation · Medical imaging

1 Introduction

Segmentation is a highly relevant task in medical imaging. Delineating organs or other regions of interest is necessary for computer-assisted diagnosis, intervention, and therapy. Manual image segmentation is a tedious, time-consuming task whose results are often subject to wide variability among users. On the other hand, fully automatic segmentation can substantially reduce the time required for target volume delineation and produce more consistent segmentation masks. Over the last several years, deep learning methods have demonstrated impressive results for segmentation tasks such as labeling tumors or various bodily structures [9, 12, 14, 22]. However, their performance comes at an enormous computational cost; training these networks to convergence can take several days on specialized computing hardware and requires a large amount of memory. These factors make 3D medical image segmentation models difficult for machine learning practitioners to use and less accessible in a clinical setting.

This study’s goal is to reduce the computational footprint of 3D segmentation models while also preserving their performance. Drawing inspiration from [11], we propose a simple modification to existing network architectures that drastically reduces the number of parameters while also largely preserving their performance. With this modification, we present a new network architecture called

PocketNet that achieves comparable segmentation performance to modern deep learning models while using less than 3% of the parameters.

1.1 Previous work

Over the last several years, there have been several attempts to cut down the number of parameters used for deep learning architectures in medical imaging segmentation. Broadly, these attempts fall into two categories: post-processing tools and architecture design strategies. More specifically, pruning, depthwise separable convolutions, and filter reductions are well-known methods to help mitigate the overparameterization of deep convolutional neural networks (CNNs) for 3D medical image segmentation [16, 19, 25]. These methods, along with their combinations, give rise to new and efficient segmentation architectures.

Introduced by LeCun et al., the main idea behind pruning is to remove the redundant connections within a neural network [16]. The process of synaptic pruning in human brains largely inspires this idea, where neural pathways form during infancy and then start to decay as we reach adulthood [6]. Likewise, when pruning an artificial neural network, we start with a sizeable pre-trained model, delete weights, and iteratively retrain the model until we notice a significant drop in performance. Within medical image segmentation, pruning reduces inference time and GPU memory while maintaining medical image segmentation performance [10, 23, 26]. However, network pruning is a post-processing step that is applied to an already existing, pre-trained network. While it is a useful tool, pruning does not solve the demands of training large, overparameterized models, which require lots of memory and high-end computing hardware.

Network architecture design strategies to reduce the number of parameters in deep neural networks for medical image segmentation include depthwise separable convolutions and reduction of the number of feature maps at each layer. Depthwise separable (DS) convolutions are a well-known tool for reducing the number of parameters associated with convolution [7, 13, 25]. DS convolution factorizes the standard convolution operation into two distinct steps: depthwise convolution followed by a pointwise convolution. A normal convolution layer has a number of parameters that is quadratic in the number of channels. In contrast, DS convolutions have a number of parameters that is linear in the number of channels. In practice, recent medical segmentation architectures take advantage of DS convolution to reduce the number of parameters in their networks by up to a factor of 5 while also achieving comparable results to conventional convolution [1, 20]. However, 3D DS convolution is not supported in standard deep learning packages and requires more memory during training due to the storage of an extra gradient layer.

By convention, the number of feature maps doubles at each layer of a U-Net style segmentation architecture. This growth in the number of feature maps accounts for a large portion of the number of training parameters. With this in mind, perhaps the simplest way to reduce overparameterization in a segmentation model is to reduce the number of feature maps. Van der Putten et al. explore this idea in [19] by dividing the number of feature maps in the decoder

portion of a U-Net by a constant factor r . For increasing values of r , the number of parameters in the decoder is reduced by up to a factor of 100, and segmentation performance remains the same. Building on the work of [19] we modify both the decoder and encoder to reduce the number of feature maps in a U-Net type architecture.

2 Materials and Methods

We propose a modification to existing network architectures that dramatically reduces the number of parameters while also retaining segmentation performance. Doubling the number of feature maps at each level of downsampling in a U-Net style architecture is the standard practice for segmentation models. However, there is no rigorous mathematical justification for this, beyond the impression that a reduction in spatial resolution due to downsampling can be offset by an increase in the number of feature maps. Yet, this strategy has been experimentally validated by numerous different architectures in the past. However, CNNs are strikingly similar to multigrid methods used for solving linear systems arising from the discretization of partial differential equations [5, 11]. When using multigrid methods, the number of features does not double at coarser grids. The number of feature maps that one uses for a finer grid (e.g., a full resolution image) is sufficient to capture the relevant information in coarser grids. Instead of doubling the number of feature maps at every level of a U-Net type architecture, we keep them constant, substantially reducing the number of parameters in our models in the process. We designate network architectures that keep the number of feature maps constant as *pocket networks*, or *PocketNets* for short, in the sense that these networks are “small enough to fit in one’s back pocket”. For example, “Pocket U-Net” refers to a U-Net architecture where we apply our proposed modification.

2.1 Network Architecture

We examine the effects of our proposed modification strategy to three widely used segmentation models - U-Net, ResNet, and DenseNet [9, 12, 14]. Each network consists of convolution block operators (blocks), a downsampling path with four max-pooling layers and an upsampling path with four transposed convolution layers. A channel-wise concatenation operation links each layer in the downsampling and upsampling paths. Figure 1 presents the overall architecture for all of the networks we test.

The differences between the three proposed architectures (U-Net, ResNet, and DenseNet) lie in the definition of each block. In a U-Net, each block consists of two convolutions. A ResNet block has two convolutions followed by an addition layer, and a DenseNet block is built with two densely connected convolutions followed by a pointwise convolution. Figure 2 provides a visual representation of the block designs for each of the architectures that we test. A ReLU activation function follows each convolution operation.

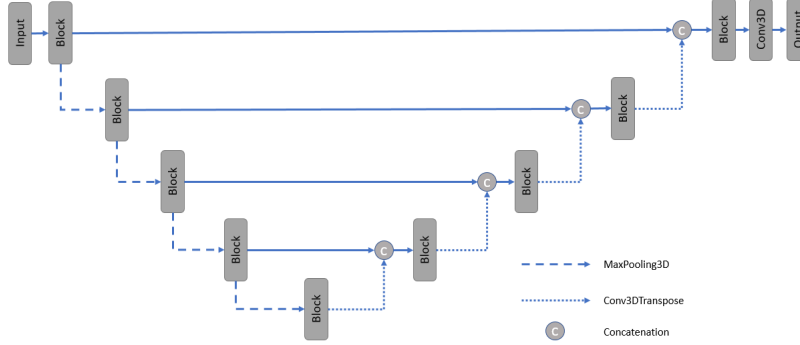


Fig. 1: Diagram of the overall architecture for each network that we test.

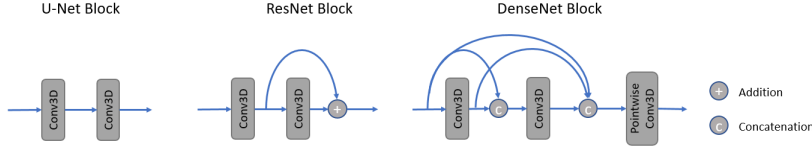


Fig. 2: Block design for U-Net (left), ResNet (center), and DenseNet (right).

2.2 Data

We test our strategy for reducing the number of parameters in image segmentation models on two publicly available datasets - the Neurofeedback Skull-stripped (NFBS) repository [18] and the Liver and Tumor Segmentation (LiTS) Challenge dataset [4]. The segmentation task for the NFBS dataset is the extraction (i.e., segmentation) of the brain from MR data; the NFBS dataset consists of 125 T1-weighted MR images with manually labeled ground truth masks. All images are provided with an isotropic voxel resolution of $1 \times 1 \times 1 \text{ mm}^3$ and are of size $256 \times 256 \times 192$. For pre-processing, we apply z-score intensity normalization and break each image into patches of size $256 \times 256 \times 5$. For the LiTS dataset, we perform liver segmentation. This dataset consists of the 131 CT scans from the MICCAI 2017 Challenge’s multi-institutional training set. These scans vary significantly in the number of slices in the axial direction and voxel resolution, although all axial slices are at 512×512 resolution. As a result of this variability, we perform 2D segmentation on the axial slices; we note that other, more sophisticated 3D methods exist to handle the LiTS data variability [4]. Each 2D slice is pre-processed by downsampling to 256×256 resolution and then windowed between -100 HU and 200 HU. During training, data augmentation is performed by randomly reflecting the slices across the sagittal plane. In contrast to the NFBS data, which uses 3D convolutions on 3D data, our LiTS data is treated as 2D only, using 2D convolutions instead.

2.3 Training and Testing

We compare each full-sized architecture’s segmentation performance to its modified counterpart. In total, we use six networks - U-Net, ResNet, and DenseNet with and without feature map doubling, for each of the NFBS and LiTS segmentation tasks. We initialize each network with 16 feature maps in the first layer. A five-fold cross-validation scheme is used to train and evaluate each architecture. We train on 80% of the images for each fold and generate validation predictions for the excluded 20%. Using this process, we create predictions on all of the images in the NFBS and LiTS datasets for each model. To evaluate a predicted segmentation mask’s validity, we use the Sorensen-Dice Similarity Coefficient (Dice) and the Hausdorff distance. Both of these metrics are available through the SimpleITK Python package [17,24]. Our loss function is calculated as an L_2 relaxation of the Dice score. During training, we use the Adam optimizer [15]. The initial learning rate is set to 0.001 and is reduced by a factor of two once learning stagnates. Training on the NFBS data uses a batch size of four for all six networks, while a batch size of 16 is used for the LiTS dataset. For each network and dataset, all network weights are initialized from a random standard normal distribution. As a post-processing step, we select the largest connected component in each predicted segmentation mask. Our models are implemented in Python using the Keras toolkit (version 2.1.6-tf) and trained on up to two NVIDIA Quadro RTX 6000 GPUs [8]. Code for each network architecture is available at github.com/aecelaya/pocketnet.

3 Results

We use the training approach described in Section 2 to obtain segmentation predictions for the NFBS and LiTS datasets, shown in Table 1 and Table 2, respectively. In both sets of segmentation results, the pocket networks achieve segmentation accuracy comparable to the full architectures while using a small fraction of the parameters; Figures 3 and 4 illustrate example predictions on the NFBS and LiTS datasets, respectively.

	# Parameters	Dice	Hausdorff (mm)	
			max	mean
DenseNet	8.1 M	0.9876	5.8785	0.0140
Pocket DenseNet	0.241 M	0.9882	5.5905	0.0131
ResNet	5.5 M	0.9865	6.4862	0.0157
Pocket ResNet	0.150 M	0.9879	6.0736	0.0137
U-Net	5.5 M	0.9844	6.6331	0.0185
Pocket U-Net	0.150 M	0.9874	5.5634	0.0141

Table 1: Dice scores and Hausdorff distances for 3D segmentation architectures for skull stripping NFBS data, with and without PocketNet modification.

	# Parameters	Dice	Hausdorff (voxels)	
			max	mean
DenseNet	626 K	0.9371	25.1669	0.4176
Pocket DenseNet	42 K	0.9317	27.5023	0.4863
ResNet	544 K	0.9363	24.3747	0.4175
Pocket ResNet	36 K	0.9303	30.5775	0.5511
U-Net	544 K	0.9338	29.7406	0.5799
Pocket U-Net	36 K	0.9285	26.1956	0.4602

Table 2: Dice scores and Hausdorff distances for 2D segmentation architectures for liver segmentation on LiTS data, with and without PocketNet modifications.

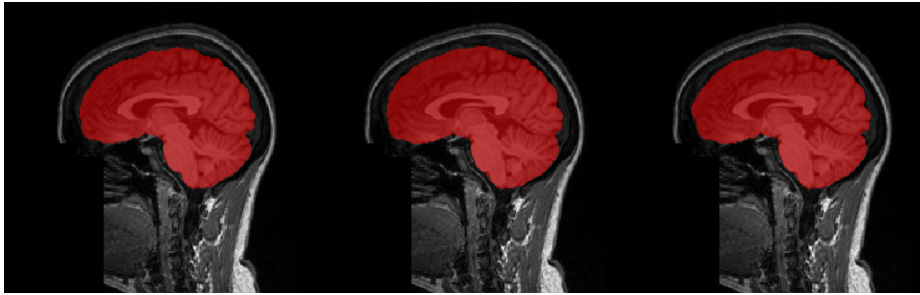


Fig. 3: An NFBS image with ground truth or predicted segmentation masks overlaid in red. Ground truth (left), DenseNet prediction (center), and Pocket DenseNet prediction (right).



Fig. 4: A LiTS image with ground truth or predicted segmentation masks overlaid in red. Ground truth (left), DenseNet prediction (center), and Pocket DenseNet prediction (right).

Among the 3D networks trained for brain segmentation on NFBS data, we observe that the DenseNet models perform better than the ResNet models, which in turn are better than the U-Net models; we observe this expected progression among both the pocket and full network architectures. For the 2D networks for liver segmentation on LiTS data, this relationship between block types holds for

Dice scores but not for the Hausdorff distance metrics, which could be explained by the anisotropic nature of the LiTS data. The difference in Dice accuracy between the pocket and full architectures for NFBS segmentations is less than or equal to 0.003, while for LiTS data it is less than or equal to 0.007 for all three block types. Boxplots of segmentation accuracy for each architecture are presented in Figures 5 and 6.

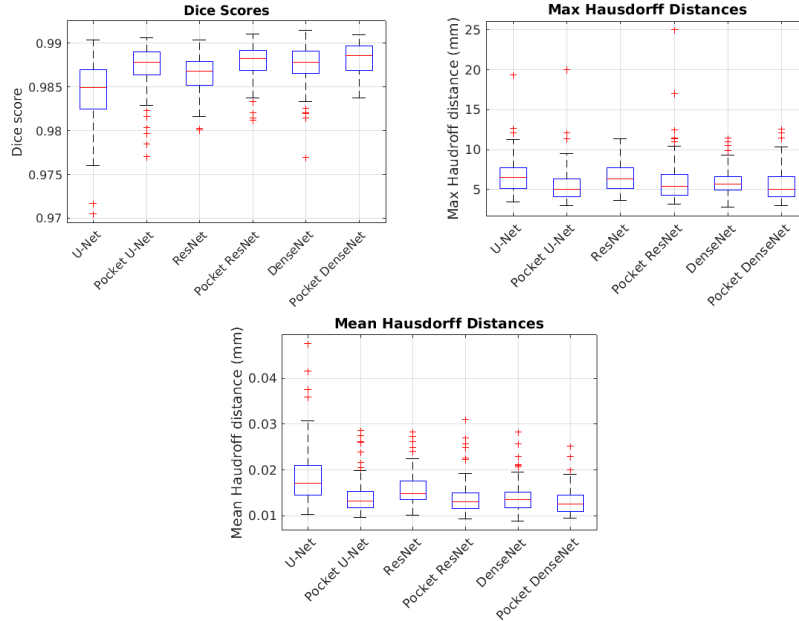


Fig. 5: Box plots of accuracy metrics for each architecture on NFBS data.

4 Discussion

When we employ our pocket networks, we observe faster training and inference times and lower memory requirements. These savings in time and memory provided by PocketNets can potentially make popular segmentation architectures more accessible in resource-constrained environments that do not have access to specialized computing hardware. However, the datasets used in this study are relatively small, and further testing on larger, more complex datasets is necessary. Furthermore, while these results are promising, additional testing is also needed to properly quantify the savings in memory and runtime that PocketNet provides. We hope to address both of these matters in future work.

Our results show that large numbers of parameters (e.g., in the millions or tens of millions) for medical image segmentation may not be necessary: comparable segmentations are achievable with substantially smaller networks, using

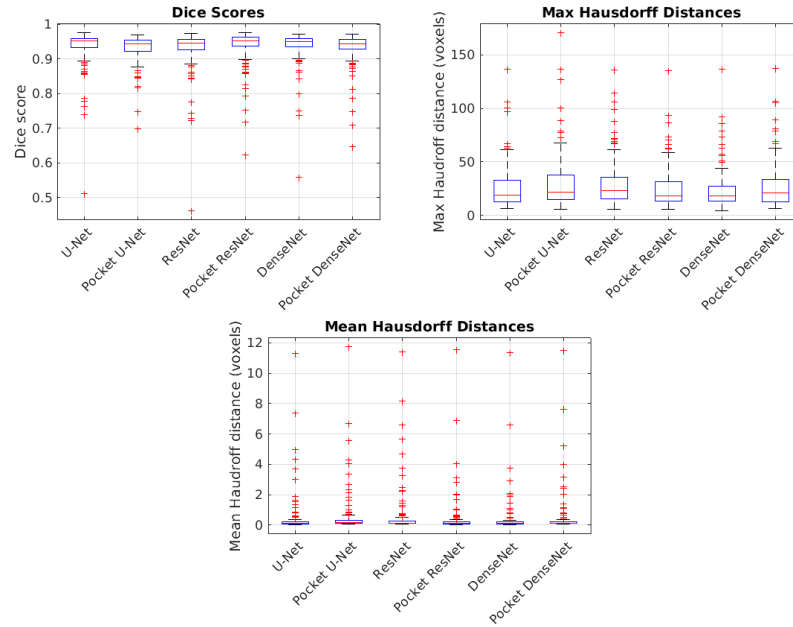


Fig. 6: Box plots of accuracy metrics for each architecture on LiTS data.

the same architectures but without doubling the number of channels at coarser resolutions. This suggests that overparameterization, which is increasingly regarded as a key feature as to why neural networks learn efficiently, might not be as critical as previously suggested [2, 3, 21]. We note that it is still possible that a small network of only 50 K parameters, such as the pocket networks for LiTS segmentation, is still overparameterized. Exactly how much overparameterization is needed to achieve the benefits suggested in the literature should be further explored.

5 Acknowledgments

Jonas Actor and Evan Gates are both supported by a training fellowship from the Gulf Coast Consortia, on NLM Training Program in Biomedical Informatics & Data Science (T15LM007093).

References

1. Alalwan, N., Abozeid, A., ElHabshy, A.A., Alzahrani, A.: Efficient 3d deep learning model for medical image semantic segmentation. *Alexandria Engineering Journal* **60**, Issue 1, 1231–1239 (2021). <https://doi.org/https://doi.org/10.1016/j.aej.2020.10.046>, <http://www.sciencedirect.com/science/article/pii/S1110016820305639>

2. Allen-Zhu, Z., Li, Y., Song, Z.: A convergence theory for deep learning via over-parameterization. In: International Conference on Machine Learning. pp. 242–252. PMLR (2019)
3. Arora, S., Cohen, N., Hazan, E.: On the optimization of deep networks: Implicit acceleration by overparameterization. In: International Conference on Machine Learning. pp. 244–253. PMLR (2018)
4. Bilic, P., Christ, P.F., Vorontsov, E., Chlebus, G., Chen, H., Dou, Q., Fu, C.W., Han, X., Heng, P.A., Hesser, J., et al.: The liver tumor segmentation benchmark (LiTS). arXiv preprint arXiv:1901.04056 (2019)
5. Bramble, J.H.: Multigrid methods. Routledge (2018)
6. Chechik, G., Meilijson, I., Ruppin, E.: Synaptic pruning in development: A computational account. *Neural Computation* **10**(7), 1759–1777 (1998). <https://doi.org/10.1162/089976698300017124>, <https://doi.org/10.1162/089976698300017124>
7. Chollet, F.: Xception: Deep learning with depthwise separable convolutions. In: Proceedings of the IEEE conference on computer vision and pattern recognition. pp. 1251–1258 (2017)
8. Chollet, F., et al.: keras (2015)
9. Çiçek, Ö., Abdulkadir, A., Lienkamp, S.S., Brox, T., Ronneberger, O.: 3d u-net: learning dense volumetric segmentation from sparse annotation. In: International conference on medical image computing and computer-assisted intervention. pp. 424–432. Springer (2016)
10. Feng-Ping, A., Zhi-Wen, L.: Medical image segmentation algorithm based on feedback mechanism convolutional neural network. *Biomedical Signal Processing and Control* **53** (2019). <https://doi.org/https://doi.org/10.1016/j.bspc.2019.101589>, <http://www.sciencedirect.com/science/article/pii/S1746809419301697>
11. He, J., Xu, J.: Mgnet: A unified framework of multigrid and convolutional neural network. *CoRR* **abs/1901.10415** (2019), <http://arxiv.org/abs/1901.10415>
12. He, K., Zhang, X., Ren, S., Sun, J.: Identity mappings in deep residual networks. In: European conference on computer vision. pp. 630–645. Springer (2016)
13. Howard, A.G., Zhu, M., end et al., B.C.: Mobilenets: Efficient convolutional neural networks for mobile vision applications. *CoRR* **abs/1704.04861** (2017), <http://arxiv.org/abs/1704.04861>
14. Huang, G., Liu, Z., Van Der Maaten, L., Weinberger, K.Q.: Densely connected convolutional networks. In: Proceedings of the IEEE conference on computer vision and pattern recognition. pp. 4700–4708 (2017)
15. Kingma, D.P., Ba, J.: Adam: A method for stochastic optimization. arXiv preprint arXiv:1412.6980 (2014)
16. Lecun, Y., Denker, J., Solla, S.: Optimal brain damage. *Advances in Neural Information Processing Systems* **2**, 598–605 (01 1989)
17. Lowekamp, B.C., Chen, D.T., Ibáñez, L., Blezek, D., Johnson, H.J.: The design of simpleitk (2013). <https://doi.org/10.3389/fninf.2013.00045>, www.frontiersin.org
18. Puccio, B., Pooley, J.P., Pellman, J.S., Taverna, E.C., Craddock, R.C.: The preprocessed connectomes project repository of manually corrected skull-stripped T1-weighted anatomical MRI data. *GigaScience* **5**(1) (10 2016). <https://doi.org/10.1186/s13742-016-0150-5>, <https://doi.org/10.1186/s13742-016-0150-5>, data available for download at: <http://preprocessed-connectomes-project.org/NFB.skullstripped/>
19. van der Putten, J., van der Sommen, F., de With, P.H.N.: Influence of decoder size for binary segmentation tasks in medical imaging. In: Išgum, I.,

- Landman, B.A. (eds.) Medical Imaging 2020: Image Processing. vol. 11313, pp. 276 – 281. International Society for Optics and Photonics, SPIE (2020). <https://doi.org/10.1117/12.2542199>, <https://doi.org/10.1117/12.2542199>
20. Qi, K., Yang, H., Li, C., et al.: X-net: Brain stroke lesion segmentation based on depthwise separable convolution and long-range dependencies. In: Medical Image Computing and Computer Assisted Intervention – MICCAI 2019. pp. 247–255. Springer International Publishing, Cham (2019)
 21. Rice, L., Wong, E., Kolter, Z.: Overfitting in adversarially robust deep learning. In: International Conference on Machine Learning. pp. 8093–8104. PMLR (2020)
 22. Ronneberger, O., Fischer, P., Brox, T.: U-net: Convolutional networks for biomedical image segmentation. In: International Conference on Medical image computing and computer-assisted intervention. pp. 234–241. Springer (2015)
 23. Weng, Y., Zhou, T., Li, Y., Qiu, X.: Nas-unet: Neural architecture search for medical image segmentation. IEEE Access **7**, 44247–44257 (2019). <https://doi.org/10.1109/ACCESS.2019.2908991>
 24. Yaniv, Z., Lowekamp, B.C., Johnson, H.J., Beare, R.: Simpleitk image-analysis notebooks: a collaborative environment for education and reproducible research (6 2018). <https://doi.org/10.1007/s10278-017-0037-8>, <https://doi.org/10.1007/s10278-017-0037-8>
 25. Ye, R., Liu, F., Zhang, L.: 3d depthwise convolution: Reducing model parameters in 3d vision tasks. CoRR **abs/1808.01556** (2018), <http://arxiv.org/abs/1808.01556>
 26. Zhou, Z., Siddiquee, M.M.R., Tajbakhsh, N., Liang, J.: Unet++: A nested unet architecture for medical image segmentation. CoRR **abs/1807.10165** (2018), <http://arxiv.org/abs/1807.10165>